

Structural distortions and model Hamiltonian parameters: from LSDA to a tight-binding description of LaMnO_3

Claude Ederer,* Chungwei Lin, and Andrew J. Millis

Department of Physics, Columbia University, 538 West 120th Street, New York, NY 10027, U.S.A.

(Dated: November 7, 2021)

The physics of manganites is often described within an effective two-band tight-binding (TB) model for the Mn e_g electrons, which apart from the kinetic energy includes also a local “Hund’s rule” coupling to the t_{2g} core spin and a local coupling to the Jahn-Teller (JT) distortion of the oxygen octahedra. We test the validity of this model by comparing the energy dispersion calculated for the TB model with the full Kohn-Sham band-structure calculated within the local spin-density approximation (LSDA) to density functional theory. We analyze the effect of magnetic order, JT distortions, and “GdFeO₃-type” tilt-rotations of the oxygen octahedra. We show that the hopping amplitudes are independent of magnetic order and JT distortions, and that both effects can be described with a consistent set of model parameters if hopping between both nearest and next-nearest neighbors is taken into account. We determine a full set of model parameters from the density functional theory calculations, and we show that both JT distortions and Hund’s rule coupling are required to obtain an insulating ground state within LSDA. Furthermore, our calculations show that the “GdFeO₃-type” rotations of the oxygen octahedra lead to a substantial reduction of the hopping amplitudes but to no significant deviation from the simple TB model.

I. INTRODUCTION

Manganite systems, $R_{1-x}A_x\text{MnO}_3$, where R is a trivalent rare earth cation (e.g. La^{3+} , Pr^{3+} , Nd^{3+} , ...) and A is a divalent alkaline earth cation (e.g. Sr^{2+} , Ca^{2+} , ...), have attracted the attention of scientists already for decades.^{1,2,3,4,5} These compounds exhibit a very rich phase diagram as a function of both temperature and composition, with various types of eventually coexisting charge, orbital, and magnetic order, and they are therefore important prototype materials to test our current understanding of correlated electron systems. In addition, the observation of “colossal magneto-resistance”,⁶ a magnetic-field induced change in electric resistivity by several orders of magnitude, has spawned further interest both in the fundamental physics behind this effect as well as in the question of whether this effect can be utilized for technological applications.

LaMnO_3 , the parent material for many manganite systems, exhibits an orthorhombically distorted perovskite structure with $Pnma$ space group (see Fig. 1a).⁸ The observed deviation from the ideal cubic perovskite structure (shown in Fig. 1b) involves both Jahn-Teller (JT) distortions of the oxygen octahedra surrounding the Mn cations,⁹ as well as a collective tilting of these octahedra, the so called “GdFeO₃-type” distortion.¹⁰ The magnetic moments of the Mn cations in LaMnO_3 order at $T_N = 140\text{ K}$ in a so-called “A-type” antiferromagnetic structure,² with parallel alignment of all moments within a certain (001) plane and antiparallel alignment of the moments between adjacent planes.

In the ideal cubic perovskite structure (see Fig. 1b) the $3d$ states of the Mn cations are split by the crystal field into the lower-lying three-fold degenerate t_{2g} states and the higher-lying two-fold degenerate e_g states. In LaMnO_3 the majority-spin t_{2g} states are fully occupied, whereas the two majority-spin e_g levels are filled with

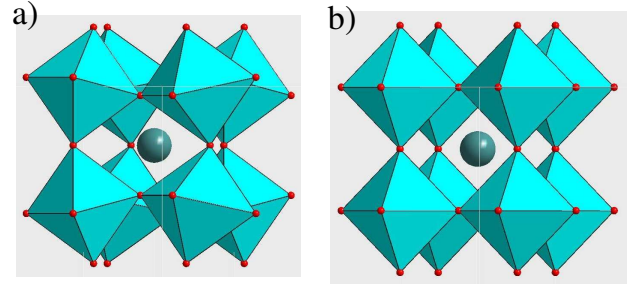


FIG. 1: a) Experimentally observed $Pnma$ structure of LaMnO_3 according to Ref. 7. b) Ideal cubic perovskite structure. The oxygen anions form a network of corner-shared octahedra. The Mn cations (not shown) are situated in the centers of the oxygen octahedra and the La cations occupy the space between the octahedra.

only one electron, according to the formal high-spin d^4 electron configuration of the Mn^{3+} cation.

The theoretical modeling of manganite systems is usually based on the assumption that the important low energy dynamics of these systems can be described within an effective two band tight-binding (TB) model for the Mn e_g electrons. In this model, electrons can hop between the e_g orbitals at neighboring Mn sites, and the corresponding kinetic energy term in the Hamiltonian is eventually complemented by local terms describing the coupling to the t_{2g} “core spin”, the coupling to the JT distortion of the surrounding oxygen octahedron, and the electron-electron interaction. These models can account for many of the properties observed in manganite systems (see Ref. 5 for a recent review). Reasonable values for the model parameters, which describe the strengths of the various competing interactions, can be inferred from experiments. Nevertheless, it is very desirable to in-

dependently calculate values for these parameters based on fundamental “first principles” theory. Evaluating the models using such independently determined parameters provides a stringent test for the accuracy of the model description.

Electronic structure calculations based on density functional theory (DFT)^{11,12} provide a way to study the ground state electronic structure of a specific material without having to resort to model assumptions, and therefore provide a good starting point for the derivation of more simplified models and their parameters (see e.g. Refs. 13 and 14). The electronic structure of LaMnO₃ has been studied previously within the local spin density approximation (LSDA) to DFT and by using the LSDA+*U* method.^{15,16,17,18} It was shown that many properties such as the correct magnetic ground state and even some spectral properties are well described by these methods, provided the correct experimental crystal structure is used in the calculation.

Although the model treatment of manganite systems usually employs a pure e_g electron description, it is generally understood that the electron hopping between the e_g states on neighboring Mn sites is truly an *effective* hopping which is mediated by the intermediate oxygen anions via d - p or d - s hopping. The resulting bands with predominant e_g character can be described by an effective two-band model if the Mn e_g states are energetically separated from the oxygen p and s states. In this case, the effective nearest neighbor hopping amplitude t between the Mn e_g states is (to leading order) given by:

$$t \propto \frac{t_{pd}^2}{E_d - E_p} . \quad (1)$$

Here, t_{pd} is the hopping amplitude between the Mn e_g and the oxygen p states, E_d and E_p are the energies of the corresponding ionic levels, and for simplicity we have neglected hopping via the oxygen s states.

The JT distortion changes the Mn-O bond lengths while the octahedral tilts change the bond angles; thus both distortions affect the overlap integrals which determine the hopping amplitude t_{pd} . It is therefore not clear *a priori* that a simple effective TB model with fixed (distortion-independent) hopping amplitudes t can be used to study the effects of lattice distortions in manganite systems.

Here, we use the Kohn-Sham band-structure calculated within the LSDA as a reference for the non-interacting TB model, and we analyze how well the relevant part of the energy dispersion of LaMnO₃ can be fitted within an effective two-band TB model for the e_g electrons. In particular, we analyze the effects of the two dominant structural distortions in LaMnO₃, the JT distortion and the GdFeO₃-type rotations, and we address the question of whether magnetic and orbital (JT) order affects the effective hopping amplitudes.

The result of our analysis is that the effective two-band model gives a good fit of the e_g -projected Kohn-Sham band-structure, provided that hopping between

both nearest and next-nearest neighbors is taken into account. We show that the same hopping amplitudes can be used for the ferromagnetic, the A-type antiferromagnetic, and the JT distorted case, so that the simple two-band TB model can be used to study the effects of JT distortions. Furthermore we quantify the dependence of the hopping amplitudes on volume changes and on GdFeO₃-type rotations. The latter lead to significant reductions of the hopping amplitudes ($\sim 25\%$ for the experimental structure) relative to the ideal cubic structure with the same unit cell volume. The hopping amplitudes corresponding to the observed bond angles should therefore be used in theoretical modeling.

Our results also provide a quantitative determination of the JT and Hund’s rule couplings. The result for the Hund’s coupling is consistent with previous work; the JT coupling is considerably smaller than previous estimates.^{19,20,21} We find that both the JT and Hund’s coupling are required to stabilize the insulating state within LSDA.

Our conclusions rely in an essential way on the energy separation of the transition metal d -bands and the oxygen p -bands; methods such as LSDA+*U* which shift the energy of the transition-metal d -bands relative to the energy of the oxygen p -bands can produce a band structure that is very poorly described by a simple two-band TB model.

The remaining part of this paper is organized as follows. Sec. II contains a brief summary of the methods and technical details of our work. We first describe the method we use for our LSDA calculations, then specify the TB Hamiltonian, and finally describe how we decompose the various structural distortions found experimentally in LaMnO₃. Our results are discussed in Sec. III, and we end with a summary of our main conclusions and implications for future work.

II. METHODS AND TECHNICAL DETAILS

A. Computational method

We calculate the LSDA Kohn-Sham band-structure for LaMnO₃ with both ferromagnetic and A-type antiferromagnetic order in various structural modifications using the projector augmented-wave (PAW) method implemented in the “Vienna Ab-initio Simulation Package” (VASP).^{22,23,24} We treat the La $5s$, La $5p$, and Mn $3p$ pseudo-core states as valence states, and we use a plane-wave energy cutoff of 400 eV in all our calculations. We employ Γ -centered $6 \times 6 \times 6$ and $4 \times 4 \times 3$ k -point grids for the calculations corresponding to the simple and quadrupled perovskite unit cells, respectively, and corresponding grids for the structures in which the unit cells are doubled along the z direction or within the x - y plane. These values result in a good convergence of the calculated band-structures.

In order to extract the bands resulting from the Mn

e_g states we use the “fatbands” technique, i.e. we assign a weight to each calculated eigenvalue, which is proportional to the amount of Mn e_g character contained in the corresponding Bloch function, and we identify the e_g -derived bands as those containing a non-negligible e_g character.

It has been shown in Ref. 15 that the LSDA gives a good overall account of the electronic properties of manganite systems, even though the tendency to open up an energy gap between occupied and unoccupied states is underestimated within the LSDA. This is a well-known feature of the LSDA, which results from the inability of the LSDA to correctly account for the strong Coulomb correlations between the rather localized d states in transition metal oxides. Such local Coulomb interactions are usually incorporated in the model Hamiltonian via a separate interaction term. In the following we do not include such an interaction term in our model analysis, and thus the corresponding deficiencies of the LSDA do not affect our results (assuming that the separate treatment of local correlations is justified), except for the question related to the energy separation between the Mn d and the oxygen p states, which is discussed in Sec. IV.

B. Model Hamiltonian

In Sec. III we relate the calculated LSDA bandstructure to the following TB model, which contains the terms that are typically used for the theoretical modeling of manganite systems (see e.g. Ref. 5):

$$\hat{H} = \hat{H}_{\text{kin}} + \hat{H}_{\text{Hund}} + \hat{H}_{\text{JT}} \quad , \quad (2)$$

with

$$\hat{H}_{\text{kin}} = - \sum_{\vec{R}, \vec{\delta}, \sigma} \mathbf{d}_{\vec{R}, \sigma}^\dagger \mathbf{t}_{\vec{R}, \vec{R} + \vec{\delta}} \mathbf{d}_{\vec{R} + \vec{\delta}, \sigma} \quad , \quad (3)$$

$$\hat{H}_{\text{Hund}} = -J \sum_{\vec{R}, a, \sigma, \sigma'} \vec{S}_{\vec{R}} \cdot \vec{\tau}_{\sigma, \sigma'} \mathbf{d}_{\vec{R}, a, \sigma}^\dagger \mathbf{d}_{\vec{R}, a, \sigma'} \quad , \quad (4)$$

$$\hat{H}_{\text{JT}} = -\lambda \sum_{\vec{R}, \sigma} \left(Q_{\vec{R}}^x \mathbf{d}_{\vec{R}, \sigma}^\dagger \boldsymbol{\tau}^x \mathbf{d}_{\vec{R}, \sigma} + Q_{\vec{R}}^z \mathbf{d}_{\vec{R}, \sigma}^\dagger \boldsymbol{\tau}^z \mathbf{d}_{\vec{R}, \sigma} \right) \quad . \quad (5)$$

Here, $d_{\vec{R}, a, \sigma}$ is the annihilation operator for an e_g electron at site \vec{R} in orbital a with spin σ , and the corresponding boldface symbol indicates a pseudo-spinor in orbital space $\mathbf{d}_{\vec{R}, \sigma} = (d_{\vec{R}, 1, \sigma}, d_{\vec{R}, 2, \sigma})^T$. The orbital indexes 1 and 2 correspond to $|3z^2 - r^2\rangle$ and $|x^2 - y^2\rangle$ orbitals, respectively. $\mathbf{t}_{\vec{R}, \vec{R} + \vec{\delta}} = \sum_{i=0}^3 t_{\vec{R}, \vec{R} + \vec{\delta}}^i \boldsymbol{\tau}^i$ are the hopping amplitudes between site \vec{R} and $\vec{R} + \vec{\delta}$ and $\boldsymbol{\tau}^i$ are the usual Pauli matrices supplemented by the 2×2 unit matrix. $\vec{S}_{\vec{R}}$ is the normalized core spin of the t_{2g} electrons ($|\vec{S}_{\vec{R}}| = 1$), and $Q_{\vec{R}}^{x,z}$ are the amplitudes of the two JT modes at site \vec{R}

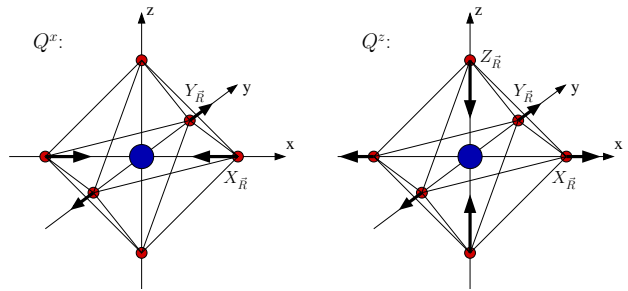


FIG. 2: Schematic depiction of the JT modes Q^x (left side) and Q^z (right side). The displacements $X_{\vec{R}}$, $Y_{\vec{R}}$, and $Z_{\vec{R}}$ used in Eqs. (6) and (7) are indicated. Since we are considering only inversion symmetric distortions of the oxygen octahedra it is enough to specify the displacements of the oxygen anions adjacent to the central Mn cation in the positive x , y , and z directions. Note that $|X_{\vec{R}}| = |Y_{\vec{R}}|$ in the case of Q^x and $|X_{\vec{R}}| = |Y_{\vec{R}}| = \frac{1}{2}|Z_{\vec{R}}|$ for Q^z .

that couple to the e_g electrons:

$$Q_{\vec{R}}^x = \frac{1}{\sqrt{2}} (X_{\vec{R}} - Y_{\vec{R}}) \quad , \quad (6)$$

$$Q_{\vec{R}}^z = \frac{1}{\sqrt{6}} (2Z_{\vec{R}} - X_{\vec{R}} - Y_{\vec{R}}) \quad . \quad (7)$$

Here, $X_{\vec{R}}$, $Y_{\vec{R}}$, and $Z_{\vec{R}}$ are the displacements along \hat{x} , \hat{y} , and \hat{z} of the oxygen anions that are situated adjacent to the Mn site at \vec{R} in x , y , and z direction, respectively, and only inversion symmetric distortions of the oxygen octahedra are taken into account (see Fig. 2). J and λ are coupling constants for the local interaction terms.

The first term in Eq. (2) describes the hopping between neighboring Mn sites. We will consider hopping between both nearest and next nearest neighbors. Symmetry dictates that the hopping matrices for nearest neighbor hopping are:

$$\mathbf{t}_{\vec{R}, \vec{R} \pm a\hat{x}} = \frac{t}{4} \begin{pmatrix} 1 & -\sqrt{3} \\ -\sqrt{3} & 3 \end{pmatrix} \quad (8)$$

$$\mathbf{t}_{\vec{R}, \vec{R} \pm a\hat{y}} = \frac{t}{4} \begin{pmatrix} 1 & \sqrt{3} \\ \sqrt{3} & 3 \end{pmatrix} \quad (9)$$

$$\mathbf{t}_{\vec{R}, \vec{R} \pm a\hat{z}} = t \begin{pmatrix} 1 & 0 \\ 0 & 0 \end{pmatrix} \quad , \quad (10)$$

and for next nearest neighbor hopping:

$$\mathbf{t}_{\vec{R}, \vec{R} \pm a\hat{x} \pm a\hat{z}} = \frac{t'}{2} \begin{pmatrix} -2 & \sqrt{3} \\ \sqrt{3} & 0 \end{pmatrix} \quad (11)$$

$$\mathbf{t}_{\vec{R}, \vec{R} \pm a\hat{y} \pm a\hat{z}} = \frac{t'}{2} \begin{pmatrix} -2 & -\sqrt{3} \\ -\sqrt{3} & 0 \end{pmatrix} \quad (12)$$

$$\mathbf{t}_{\vec{R}, \vec{R} \pm a\hat{x} \pm a\hat{y}} = \frac{t'}{2} \begin{pmatrix} 1 & 0 \\ 0 & -3 \end{pmatrix} \quad . \quad (13)$$

Here, a is the lattice constant of the underlying cubic perovskite lattice.

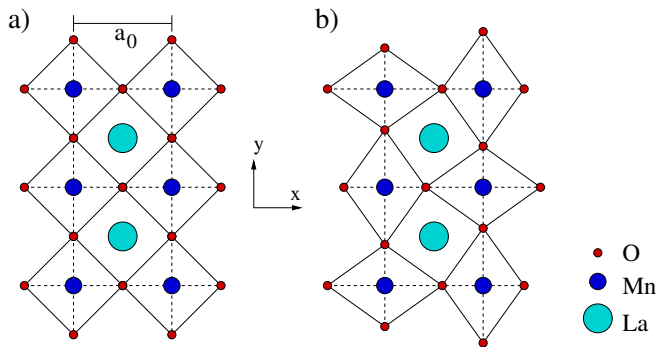


FIG. 3: Staggered Q^x -type JT distortion within the x - y plane found experimentally in LaMnO_3 . The long and short axes of the octahedra alternate along the x and y directions, as shown in b), compared to the ideal structure shown in a).

The second and third terms in Eq. (2) describe the Hund’s rule coupling to the t_{2g} core spin and the coupling to the JT distortion of the oxygen octahedra surrounding site \vec{R} , respectively. The normalized t_{2g} core spin is treated as a classical vector which is fixed externally in our model calculations. The values of $Q_{\vec{R}}^{x/z}$ are given by the positions of the oxygen anions used in our LSDA calculations and are also treated as external parameters in the TB model.

C. Structural decomposition

As described in the introduction, LaMnO_3 exhibits a strongly distorted perovskite structure with space group $Pnma$.⁸ The deviation of this structure from the perfect cubic perovskite structure (with space group $Pm\bar{3}m$) can be decomposed into the following three contributions:

- (i) A staggered (checkerboard-like) Q^x -type JT distortion of the oxygen octahedra within the x - y plane, with the long and short axes of neighboring octahedra alternating between the x and y directions (see Fig. 3). This JT distortion leads to a doubling of the unit cell compared to the ideal cubic perovskite structure, with new “in-plane” lattice vectors $\vec{a} = a_0(\hat{x} - \hat{y})$ and $\vec{b} = a_0(\hat{x} + \hat{y})$, where a_0 is the lattice constant of the original (undistorted) perovskite structure. Identical x - y planes are stacked on top of each other along the z direction. The resulting symmetry is tetragonal.
- (ii) “GdFeO₃-type” rotations (tilting) of the oxygen octahedra, leading to an additional doubling of the unit cell along the z direction, with the new lattice vector $\vec{c} = 2a_0\hat{z}$, and a reduction to orthorhombic $Pnma$ symmetry.
- (iii) Displacements of the La cations, and a deformation (strain) of the parallelepiped formed by the lattice

TABLE I: Decomposition of the experimentally observed distortion of the oxygen network into JT component and GdFeO₃-type (GFO) rotations. The upper four lines contain the Wyckoff positions of the two inequivalent oxygen sites O1 (4c) and O2 (8d) in the experimental structure (Ref. 7), in the ideal cubic perovskite structure (note that these values correspond to a quadrupled unit cell), and our decomposition in pure JT and pure GdFeO₃-type components. $\Delta\vec{r}$, $\Delta\vec{r}_{\text{JT}}$, and $\Delta\vec{r}_{\text{GFO}}$ represent the corresponding full experimental distortion, and its decomposition into pure JT and GFO-type distortion, respectively. x , y , and z are the coordinates with respect to the orthorhombic lattice vectors.

	O1 (4c)			O2 (8d)		
	x	y	z	x	y	z
Exp. (Ref. 7)	-0.0733	-0.0107	0.25	0.2257	0.3014	0.0385
Ideal	0.0	0.0	0.25	0.25	0.25	0.0
JT	0.0	0.0	0.25	0.2636	0.2636	0.0
GFO	-0.0733	-0.0107	0.25	0.2122	0.2879	0.0385
$\Delta\vec{r}$	-0.0733	-0.0107	0.0	-0.0243	0.0514	0.0385
$\Delta\vec{r}_{\text{JT}}$	0.0	0.0	0.0	0.0136	0.0136	0.0
$\Delta\vec{r}_{\text{GFO}}$	-0.0733	-0.0107	0.0	-0.0379	0.0379	0.0385

vectors \vec{a} , \vec{b} , and \vec{c} , consistent with the orthorhombic crystal class.

We expect that the internal distortions of the oxygen network, i.e. components (i) and (ii) described above, have the largest effect on the e_g bands of LaMnO_3 via the ligand-field splitting, whereas the influence of the lattice strain and of the La displacements, i.e. component (iii), can be neglected. We test the validity of this hypothesis in Sec. III A.

In the following, except for the test calculations presented in Sec. III A, we therefore consider only components (i) and (ii). This means that we use the “pseudo-cubic” lattice vectors \vec{a} , \vec{b} , and \vec{c} defined above, discarding any orthorhombic strain, and we place the La cations on their ideal positions, corresponding to the perfect cubic perovskite structure. For the internal distortion of the oxygen network, we use the experimental data obtained in Ref. 7, which we decompose into the pure JT distortion and the GdFeO₃-type distortion, as described below. Furthermore, we use a “cubic” lattice constant $a_0 = 3.9345$ Å, which results in the same volume per formula unit as in the experimentally observed structure.⁷

Table I lists the Wyckoff positions for the two inequivalent oxygen sites O1 (4c) and O2 (8d) in the experimentally determined $Pnma$ structure,⁷ and how we decompose the corresponding structural distortion in the pure JT component (i) and the GdFeO₃-type distortion (ii). The decomposition is such that $\Delta\vec{r} = \Delta\vec{r}_{\text{JT}} + \Delta\vec{r}_{\text{GFO}}$ and $\Delta\vec{r}_{\text{JT}}$ is orthogonal to $\Delta\vec{r}_{\text{GFO}}$, where $\Delta\vec{r}$, $\Delta\vec{r}_{\text{JT}}$, and $\Delta\vec{r}_{\text{GFO}}$ are the full experimental distortion and its decomposition into pure JT and GdFeO₃-type distortion, respectively. Since the Wyckoff coordinates x , y , and z can be directly interpreted as the coordinates relative

to the lattice vectors \vec{a} , \vec{b} , and \vec{c} , it follows that in the purely JT distorted structure each oxygen anion O2 is displaced by $|\Delta\vec{r}_{\text{JT}}(\text{O2})| = |\Delta x_{\text{JT}}(\text{O2})\vec{a} + \Delta y_{\text{JT}}(\text{O2})\vec{b} + \Delta z_{\text{JT}}(\text{O2})\vec{c}| = 0.1070 \text{ \AA}$. According to Eq. (6) this corresponds to a JT amplitude of $Q_0^z = 0.1513 \text{ \AA} = 0.0385 a_0$.

III. DISCUSSION OF RESULTS

A. Test of structural decomposition

In the previous section we stated that only components (i) and (ii), i.e. the internal distortion of the oxygen network, are important for the e_g bands in LaMnO_3 , and that the lattice strain as well as the displacements of the La cations are negligible. In order to test this hypothesis, we now compare the LSDA band-structure calculated for the full experimental structure of Ref. 7 with the one calculated for the slightly simplified structure described above, where the lattice strain and the La displacements are set to zero, while the internal coordinates of the oxygen anions are the same as observed experimentally.

The corresponding LSDA band-structures in the energy range of the Mn e_g bands calculated for A-type antiferromagnetic ordering are shown in Fig. 4 along certain high symmetry directions of the orthorhombic Brillouin zone. The Mn e_g bands are visualized by dots along the bands, with the radius of the dots proportional to the amount of Mn e_g character contained in the corresponding Bloch-function. It is clearly seen that the band-structures obtained for the fully experimental structure and for the simplified structure with only the oxygen distortions included are nearly indistinguishable, with only small deformations of the energy bands resulting from the orthorhombic strain and the La displacements. This validates our initial hypothesis, and in the following we therefore analyze only the effect of the internal structural distortion of the oxygen octahedra on the dispersion of the e_g bands.

We point out that by setting the lattice strain to zero we also neglect any homogeneous Q^z -type JT distortion. The good agreement between the two band-structures shown in Fig. 4 thus also indicates that there is no noticeable effect of Q^z on the electronic band-structure of LaMnO_3 in its experimental crystal structure.

The simplified structure that gives rise to the LSDA band-structure shown in the bottom part of Fig. 4 results from the superposition of distortions (i) and (ii) (described above) of the oxygen network. In the following we will first establish the e_g band-structure of LaMnO_3 in the ideal cubic perovskite structure and then separately introduce either the JT distortions, component (i), or the GdFeO_3 -type rotations, component (ii), and analyze the corresponding effects on the e_g bands.

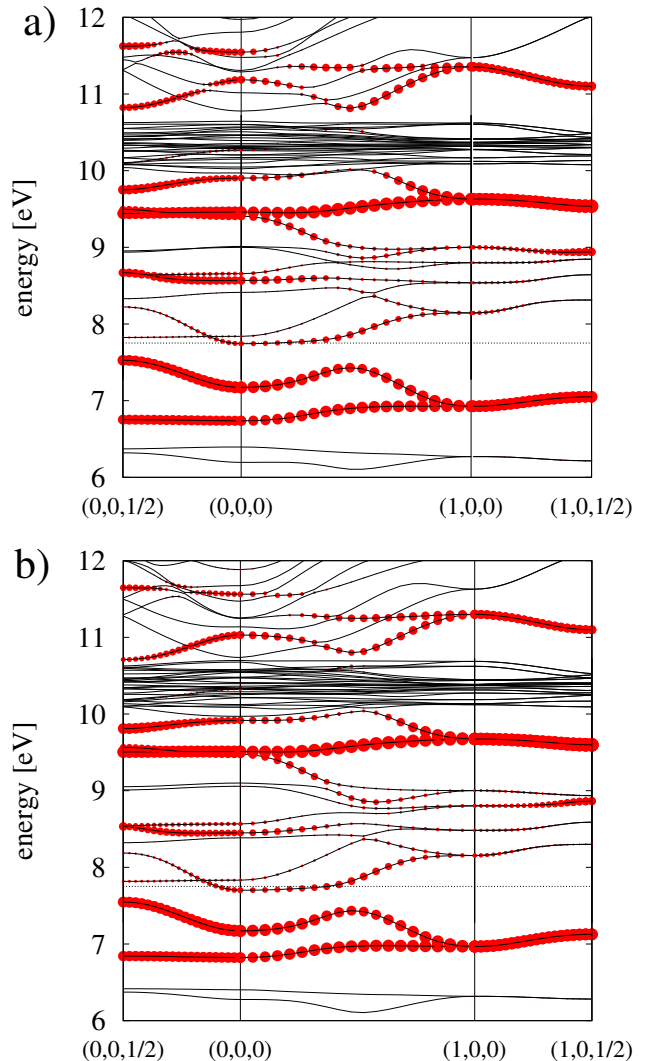


FIG. 4: LSDA energy bands (thin lines) along high symmetry directions of the orthorhombic Brillouin zone calculated for a) the exact experimental structure, and b) for the simplified structure with no orthorhombic strain and the La cations on their ideal positions. Both calculations are done for A-type antiferromagnetic ordering. The thick dots indicate the amount of Mn e_g character in the corresponding Bloch functions. The dashed horizontal line at $\sim 7.75 \text{ eV}$ indicates the Fermi energy. In b) the high symmetry k -points are given in cartesian coordinates and in units of π/a_0 , in a) the corresponding k -points are labeled identically but correspond to the slightly strained reciprocal lattice of the experimental structure. The two cases are nearly indistinguishable.

B. Cubic structure

Fig. 5 shows the calculated LSDA energy dispersion around the Fermi-level, calculated for ferromagnetic cubic LaMnO_3 in the undistorted cubic perovskite structure with $a_0 = 3.9345 \text{ \AA}$. Only the majority spin bands are shown. Within the TB model defined in Eq. (2),

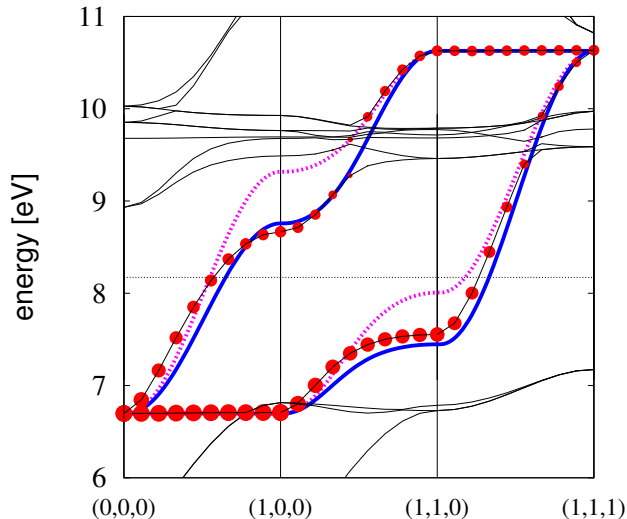


FIG. 5: Majority spin bands for cubic ferromagnetic LaMnO_3 . The LSDA band-structure is represented by thin lines, with the dots indicating the amount of Mn e_g character in the corresponding Bloch function. The thick broken line is the TB fit with only nearest neighbor hopping, whereas the thick solid line represents the TB fit including both nearest and next nearest neighbor hopping. The thin dashed horizontal line at ~ 8.2 eV indicates the Fermi energy. The high symmetry k-points are given in cartesian coordinates and in units of π/a_0 .

the Hund's coupling simply splits the spin majority and minority bands rigidly by $\Delta E = 2J$ for a ferromagnetic arrangement of the t_{2g} core spins, and we therefore discuss only the majority spin bands in the following. The Mn e_g bands are again visualized by the dots along the bands in Fig. 5. It is evident that even though the Mn e_g bands are intersected by other bands, the e_g dispersion can be nicely traced along the dots. The e_g bands are about half-filled, as expected from the formal electron configuration $t_{2g}^3 e_g^1$ of the Mn^{3+} ion. The bands at ~ 7 eV and lower, just touching the lower range of the e_g bands, are the filled majority Mn t_{2g} bands. The weakly dispersive bands slightly below 10 eV that intersect the Mn e_g bands correspond to the La $4f$ states, and the strongly dispersive unoccupied bands above the Mn e_g manifold have predominantly La d character.

The thick lines in Fig. 5 correspond to fits of the nearest and next nearest neighbor TB models for the e_g bands. The nearest neighbor hopping parameter $t = 0.655$ eV is determined from the full e_g bandwidth $W = 3.928$ eV = $6t$. The next nearest neighbor hopping parameter t' is obtained in the following way: In the next nearest neighbor model the width of the energy dispersion of the upper e_g band between k-points $\Gamma = (0, 0, 0)$ and $X = (1, 0, 0)$ is equal to $\Delta E_{\Gamma X}^{(2)} = 4t - 16t'$, whereas the dispersion width of the lower band between X and $M = (1, 1, 0)$ is equal to $\Delta E_{XM}^{(1)} = 2t - 16t'$.²⁵ The corre-

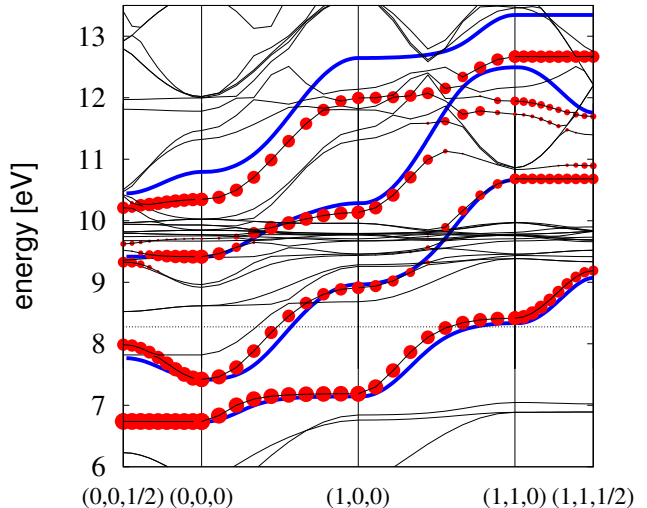


FIG. 6: Band-structure for cubic LaMnO_3 with A-type antiferromagnetic order. The LSDA band-structure is represented by thin lines, with the dots indicating the amount of Mn e_g character in the corresponding Bloch function. The thick line represents the TB fit including both nearest and next nearest neighbor hopping. The thin dashed horizontal line at ~ 8.3 eV indicates the Fermi energy. The high symmetry k-points are given in cartesian coordinates and in units of π/a_0 .

sponding energy differences obtained from the LSDA calculation are $\Delta E_{\Gamma X}^{(2)} = 0.851$ eV and $\Delta E_{XM}^{(1)} = 1.965$ eV, leading to $t' = 0.041$ eV or $t' = 0.029$ eV, respectively (and using the previously obtained $t=0.655$ eV). An average value of $t' = 0.035$ eV is used for the TB fit in Fig. 5 and in the remaining part of this paper.

It becomes clear from Fig. 5 that the simple nearest neighbor TB model cannot reproduce the LSDA dispersion very well, whereas the next nearest neighbor TB model leads to a very good description of the energy dispersion for all k-points.

We point out that a nonmagnetic LDA calculation results in a low-spin electron configuration and the loss of the t_{2g} core spin. Indeed, if we perform a nonmagnetic LDA calculation, the e_g bands are empty and higher in energy compared to the oxygen p levels, which in accordance with Eq. (1) results in a reduced bandwidth of 3.546 eV, corresponding to a nearest neighbor hopping amplitude of $t = 0.591$ eV. A nonmagnetic LDA calculation is thus not necessarily a good representation of the electronic structure of the paramagnetic phase, and we therefore use the ferromagnetic state as the starting point for the model analysis. In general, this shows that an LDA+DMFT treatment of LaMnO_3 based on a nonmagnetic LDA calculation, such as the one presented in Ref. 27, leads to a slight underestimation of the electron hopping.

Next we investigate the influence of A-type antiferromagnetic order. Fig. 6 shows the calculated LSDA band-

structure for this case. Note that the underlying crystal structure is still perfect cubic perovskite. Again, the e_g character of the bands is visualized by the dots. The thick lines corresponds to the fit within our antiferromagnetic next nearest neighbor TB model with the hopping parameters obtained from the ferromagnetic case. Due to the doubling of the magnetic unit cell the number of bands is also doubled. A Hund's-rule parameter $J = 1.340$ eV is obtained from the energy splitting at the Γ point between the two bands at 6.7 eV and 9.4 eV, which show no dispersion along $\bar{\Gamma}A$ ($A = (0, 0, 1/2)$). This splitting is exactly equal to $2J$ in the TB model. The value $J = 1.340$ eV is within 2.4% of the value $J = 1.309$ eV obtained from the ferromagnetic band-structure as the splitting between majority and minority spin states at the Γ point (not shown).

Fig. 6 shows that the two lowest e_g bands are described very well by the antiferromagnetic TB model. The upper two bands show some deviations from the model, especially in the high energy region. This is an inevitable result of the description within a pure d band model. As described in Sec. I, the "true" hopping is mediated by the oxygen p orbitals and therefore the e_g dispersion depends on the energetic distance from the oxygen p levels (see Eq. (1)). This leads to a slight overestimation of the energy dispersion for the high energy states in the pure d model. The same effect can also be observed in the ferromagnetic case: Due to their higher energy relative to the oxygen p states, the bandwidth of the e_g minority spin bands is smaller than for the corresponding majority spin bands. The nearest neighbor hopping parameter corresponding to the minority spin bands in the ferromagnetic case is $t = 0.548$ eV. In the following we use the value $t = 0.655$ eV, corresponding to the majority spin bands in the ferromagnetic configuration, since this value is representative for the e_g bands close to the Fermi level which determine the important low energy behavior in manganite systems.

Fig. 7 shows the dependence of both nearest and next nearest hopping parameters on the lattice constant a . The nearest neighbor hopping t decreases with increasing Mn-O bond length, whereas the next nearest neighbor hopping t' shows a slight increase. This somewhat unexpected behavior of t' results from the fact that the energy difference between oxygen p and Mn d states decreases with increasing volume, and therefore counteracts the effect of the reduced overlap integrals for larger lattice constants.

C. Purely JT distorted structure

We now address the effect of the JT distortion of the oxygen octahedra on the e_g bands in LaMnO_3 . As described in Sec. II C, we consider only the internal distortions of the oxygen network. This means that we displace the oxygen anions relative to the cubic structure according to the decomposition of the Wyckoff posi-

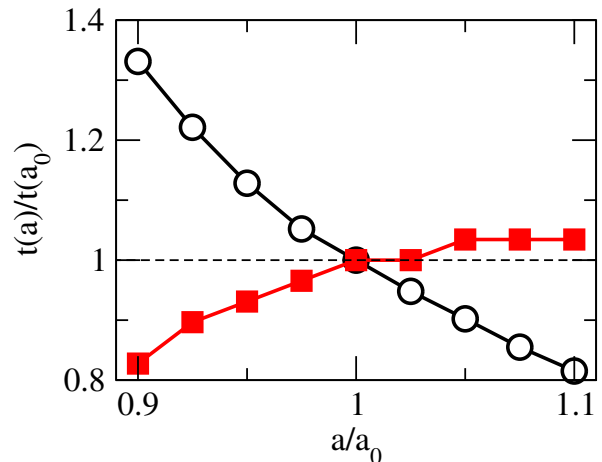


FIG. 7: Variation of hopping amplitudes with lattice constant. Open circles correspond to the nearest neighbor hopping t and filled squares correspond to the next nearest neighbor hopping t' . a_0 indicates the lattice constant derived from the experimental unit cell volume.

tions described in Table I (line "JT"). This results in the staggered arrangement of JT distorted oxygen octahedra shown in Fig. 3b, with the same JT amplitude Q_0^x as in the experimental structure.

Fig. 8 shows the calculated LSDA majority spin bands for LaMnO_3 in the purely JT distorted structure with ferromagnetic spin ordering. Due to the unit cell doubling within the x - y plane compared to the cubic structure, the two bands corresponding to the k -points between $X = (1, 0, 0)$ and $M = (1, 1, 0)$ in the ferromagnetic cubic case (see Fig. 5) are "back-folded" between the k -points $U = (1, 0, 0)$ and $\Gamma = (0, 0, 0)$ in the tetragonal Brillouin zone. In addition, the two bands between $M = (1, 1, 0)$ and $R = (1, 1, 1)$ in Fig. 5 now correspond to the two upper bands between $\Gamma = (0, 0, 0)$ and $Z = (0, 0, 1)$ in Fig. 8, and the two bands between $U = (1, 0, 0)$ and $R = (1, 0, 1)$ in Fig. 8 are now twofold degenerate. It can be seen that the level splitting between the two original e_g states at the Γ point (at ~ 6.7 eV in Fig. 8), which are degenerate in the cubic case, is very small (~ 0.08 eV), and that the main effect of the JT distortion is to remove the band crossing between Γ and $U = (1, 0, 0)$, resulting from the simple "back-folding" of the cubic band-structure due to the unit cell doubling.

To obtain the value of the JT coupling constant λ within our TB model, we first determine the k -point of the band crossing between Γ and U for the case of zero JT distortion. We then determine λQ_0^x in the model by fitting the splitting at this k -point to the corresponding splitting obtained from the LSDA calculation. In this way we obtain a value of $\lambda Q_0^x = 0.248$ eV, corresponding to $\lambda = 1.639$ eV/ \AA , since $Q_0^x = 0.1513$ \AA (see Sec. II C). Alternatively we can also fit the small splitting of the two lowest e_g bands at the Γ point by numerically adjusting the JT coupling. In this way we find $\lambda Q_0^x = 0.289$ eV,

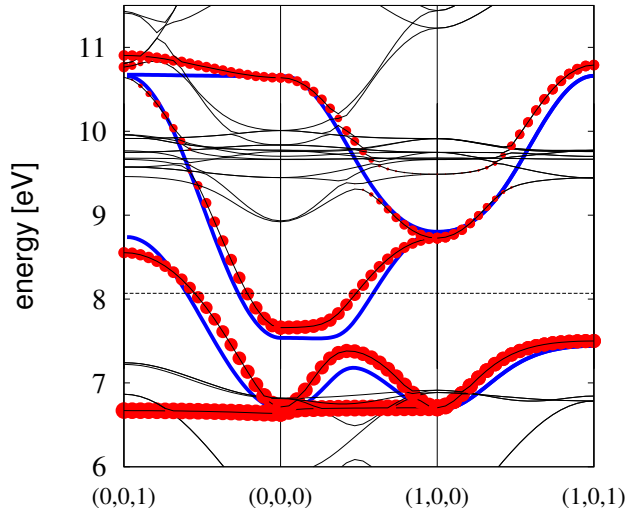


FIG. 8: Majority-spin band-structure for ferromagnetic LaMnO₃ in the purely JT distorted structure (see Fig. 3b), where the unit cell is doubled in the x - y -plane. The high symmetry k -points are given with respect to the cartesian coordinate system defined by the reciprocal lattice vectors of the undistorted cubic structure. The units are π/a_0 . The LSDA band-structure is represented by thin lines with the dots indicating the amount of Mn e_g character in the corresponding Bloch function. The thick line represents the TB fit and the thin dashed horizontal line at ~ 8.1 eV indicates the Fermi energy.

corresponding to $\lambda = 1.910 \text{ eV}/\text{\AA}$, which is within 17% of the value obtained above. This shows that the extracted coupling strength does not depend critically on the fitting procedure.

The energy dispersion calculated within the TB model using the hopping amplitudes $t = 0.655 \text{ eV}$ and $t' = 0.035 \text{ eV}$ obtained for the cubic structure and the JT coupling constant $\lambda = 1.639 \text{ eV}/\text{\AA}$ obtained in the way described above is compared to the full LSDA band-structure in Fig. 8. It can be seen that the dispersion of the e_g -projected bands is well described within the TB model. Some deviations occur close to the lifted band crossing between Γ and $U = (1, 0, 0)$. These deviations are most likely caused by the asymmetry of the Mn-O bonds, which is neglected in the effective e_g TB model. The good overall quality of the TB fit shows that the TB hopping amplitudes are not affected by the presence of the JT distortion. This indicates that the model description with the assumed local coupling of the JT distortion to the e_g levels is justified.

To test whether the linear form of the coupling term within our model is consistent with the density functional theory calculation, and to further test our procedure for obtaining λQ^x from the LSDA results, we perform additional calculations with different amplitudes of the JT distortion. The results are presented in Fig. 9, where the JT energy λQ_0^x is determined by fitting the band-splitting

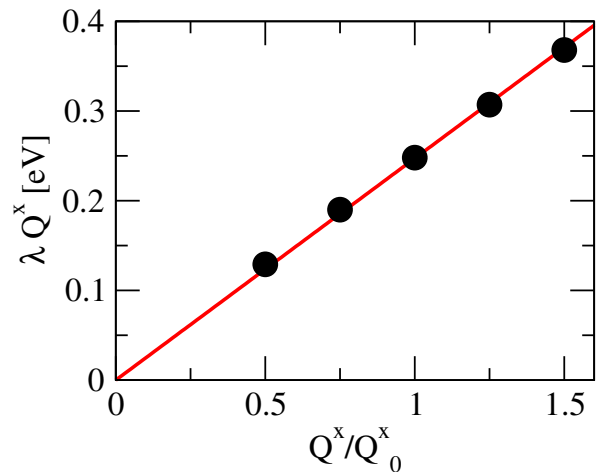


FIG. 9: Magnitude of λQ^x obtained by fitting the TB model to LSDA calculations with different amplitudes of the JT distortion. Q_0^x indicates the magnitude of the JT distortion found in the experimental structure. Filled circles are the results of the actual calculations, whereas the straight line corresponds to $\lambda Q^x = 0.247 \text{ eV } Q^x/Q_0^x$.

between Γ and $U = (1, 0, 0)$. We note that λQ^x on the ordinate in Fig. 9 should be regarded as the model parameter that we obtain by our fitting procedure, whereas the abscissa Q^x/Q_0^x characterizes the input structure for our LSDA calculation (relative to the experimentally observed JT distortion Q_0^x). It is evident that the dependence of λQ^x on the input distortion is nearly perfectly linear, which indicates the good quality of our fit and the adequacy of the linear coupling term within the model.

It becomes clear from Fig. 8 that the JT distortion in the experimentally observed structure of LaMnO₃ has only a weak effect on the dispersion along k_z . This is complementary to the effect of the A-type magnetic order, which strongly suppresses the electron hopping along this direction. The insulating band-structure obtained in LSDA for the fully distorted structure with A-type antiferromagnetic order is therefore a combined effect of both the staggered JT distortion within the x - y plane and the A-type antiferromagnetism. To achieve an insulating state within LSDA solely due to the JT distortion (i.e. for the ferromagnetic case), would require an unrealistically large JT amplitude. Within our TB model, a value of $\lambda Q^x > 1.1 \text{ eV}$, i.e. more than four times the JT distortion of the experimental structure, is required to open up an energy gap. This is due to the large value of the hopping t and the fact that for staggered JT order H_{JT} does not commute with H_{kin} . The fact that the JT distortion alone is not enough to stabilize an insulating state in LaMnO₃ has also been pointed out in Refs. 19,21,28.

One possibility for explaining the insulating character of LaMnO₃, as noted by previous authors,¹⁹ is that electron-electron interactions beyond LSDA increase the effective JT splitting, thereby stabilizing the insulating

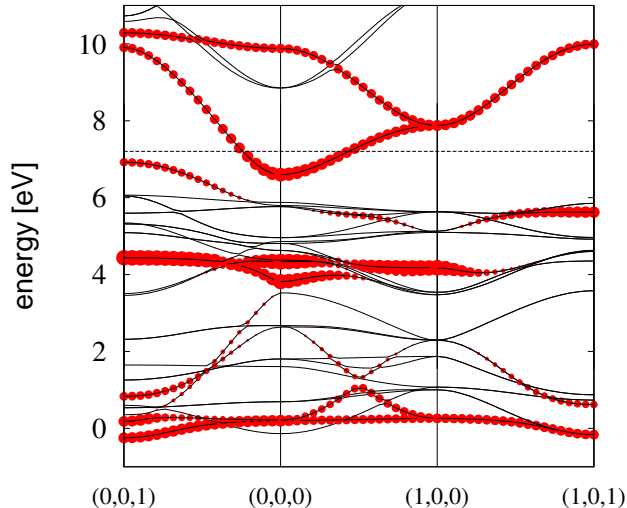


FIG. 10: Majority-spin band-structure for ferromagnetic LaMnO₃ in the purely JT distorted structure calculated using the LSDA+ U method with $U_{\text{eff}} = 7.12$ eV ($U = 8$ eV and $\mathcal{J}^H = 0.88$ eV). The high symmetry k -points are given in cartesian coordinates and in units of π/a_0 . The Kohn-Sham band-structure is represented by thin lines with the dots indicating the amount of Mn e_g character in the corresponding Bloch function. The thin dashed horizontal line at ~ 7.2 eV indicates the Fermi energy. The overlapping bands in the energy range between 0 eV and 6 eV have mixed O $2p$ -Mn $3d$ character.

state. To address this we have performed additional LSDA+ U calculations (which will be discussed in detail elsewhere). In the LSDA+ U method, the interactions between the d states of the transition metal cations are treated explicitly on the level of a mean-field Hubbard model.²⁹ Thereby, a parameter U represents the strength of the (screened) on-site Coulomb repulsion between the d electrons and a parameter \mathcal{J}^H represents the Hund's coupling. In our LSDA+ U calculations we use a slightly simplified approach where only $U_{\text{eff}} = U - \mathcal{J}^H$ enters.³⁰

We expect that the on-site Coulomb repulsion enhances the effect of the JT distortion and therefore drives the system towards an insulating state as the value of U is increased. However, the calculated LSDA+ U band-structure for the purely JT distorted case with $Q^x = Q_0^x$ and ferromagnetic spin order stays metallic even for a rather large Hubbard parameter of $U = 8$ eV (see Fig. 10). The reason for this is the following: The use of the LSDA+ U method leads to a strong downward energy shift of the occupied part of the e_g bands and also to a moderate overall downshift of the d states as a whole. As a result of the latter, the higher-lying, mostly unoccupied e_g bands in LaMnO₃ move somewhat closer to the O $2p$ bands, which are located in the energy range between 0 eV and 6 eV and are not shifted within the LSDA+ U method. Furthermore, the strong downward shift of the occupied d bands results in an energetic over-

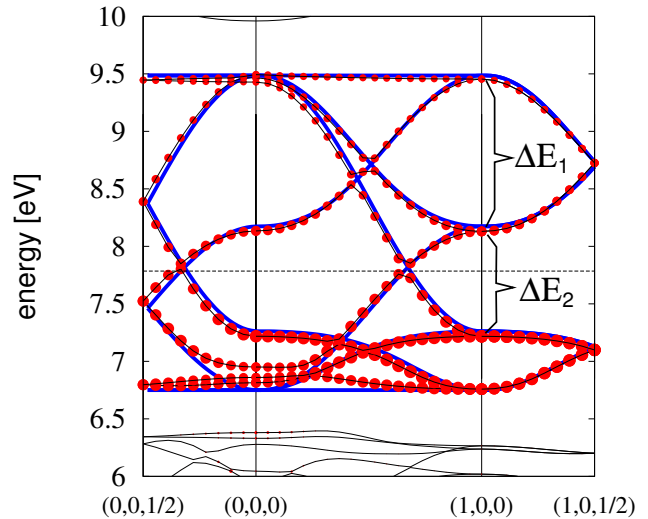


FIG. 11: LSDA energy bands (majority spin) for ferromagnetic LaMnO₃ with the experimentally observed GdFeO₃-type tilting of the oxygen octahedra, but without JT distortion. The LSDA band-structure is represented by thin lines with the dots indicating the amount of Mn e_g character in the corresponding Bloch function. The thick line represents the TB fit with reduced hopping amplitudes and the thin dashed horizontal line at ~ 7.8 eV indicates the Fermi energy. The high symmetry k -points are given in cartesian coordinates and in units of π/a_0 . ΔE_1 and ΔE_2 mark the energy differences plotted in Fig. 12.

lap and therefore strong hybridization between the occupied e_g states and the O $2p$ bands. In this case the simple two-band TB model is not applicable any more, and some mixed p - d bands, which extend above the original top of the O $2p$ states at 6 eV, reach above the Fermi level. Since the LSDA+ U method corrects only for the Coulomb interactions between the Mn d states, it is not obvious whether this shift of the d states relative to the O $2p$ states is a real physical effect or rather an artifact of the LSDA+ U method (see Sec. IV for a further discussion of this point). An exact experimental determination of the energy separation between the Mn d and O p states in LaMnO₃ would provide further insight on this.

D. GdFeO₃-type rotations

Finally, we address the effect of the GdFeO₃-type oxygen octahedra rotations. These distortions change the Mn-O-Mn bond angles and are therefore expected to alter the magnitude of the hopping amplitudes. In addition, due to the resulting symmetry lowering, this distortion will enable hopping between orbitals that was either symmetry-forbidden or negligibly small in the undistorted state.

Fig. 11 shows the calculated LSDA energy bands for the structure where only the GdFeO₃-type distortion,

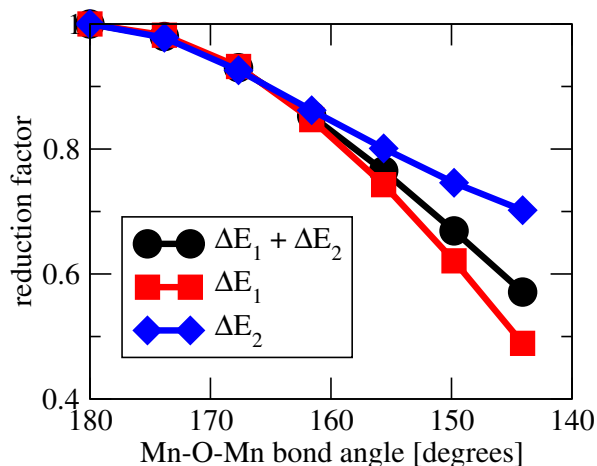


FIG. 12: Reduction of some characteristic energy differences at the k -point $U = (1, 0, 0)$ (see Fig. 11) for different amplitudes of the GdFeO₃-type distortion, which are indicated by the corresponding Mn-O-Mn bond angle.

component (ii) in Sec. II C, is included, whereas the JT distortion, component (i), is set to zero. The Wyckoff positions of the oxygen anions for this configuration are listed in Table I (line “GFO”). In this structure the Mn-O-Mn bond angles are reduced from the ideal 180° to about 155°. The thick line in Fig. 11 corresponds to a fit within the next-nearest neighbor TB model with both nearest and next-nearest hopping amplitudes scaled by a factor of 0.7 compared to the perfectly cubic case. The high quality of the fit is striking, even though the LSDA band structure shows some additional dispersion at the bottom of the e_g bands which is not accounted for in the TB model. It appears that, to a good accuracy, the oxygen tilts can be incorporated in the model simply by reducing the hopping amplitudes in an appropriate way without having to include additional hopping parameters due to the lower symmetry.

To further quantify the reduction of the hopping amplitudes as a result of the GdFeO₃-type distortion, we perform calculations for different degrees of distortion, by scaling $\Delta\vec{r}_{\text{GFO}}$ (see Table I) accordingly. Fig. 12 shows the resulting reduction of some characteristic energy differences at the k -point $U = (1, 0, 0)$ as a function of the Mn-O-Mn bond angle. If the GdFeO₃-type rotations would lead to a simple scaling of the undistorted band-structure, all the lines in Fig. 12 would fall on top of each other. It can be seen that this is in fact a good approximation for Mn-O-Mn bond angles down to $\sim 155^\circ$, which corresponds to the experimentally observed structure of LaMnO₃. For bond angles smaller than 155° the band-structure starts deviating more significantly from the cubic case due to new hopping paths that become allowed in the distorted structure.

IV. SUMMARY AND CONCLUSIONS

In summary, we have shown, by comparing LSDA band-structure calculations to simple TB models, that the relevant electronic states in LaMnO₃ are well described by a model of e_g orbitals with nearest and next-nearest neighbor hoppings. We have quantified the effect of changes in bond length (Fig. 7) and of the octahedral rotations (Fig. 12) on the hopping parameters, and we find that for physically relevant values (bond angles $\gtrsim 155^\circ$) the GdFeO₃-type rotations significantly change the value of the hopping parameters but do not invalidate the TB description. Of particular importance is our finding that both the JT lattice distortions and the Hund’s rule coupling are quantitatively accounted for by adding on-site interactions to the TB model, *without* changing the hopping parameters. In summary, these results justify a TB plus interaction description of manganite systems, and suggests more generally that such a description is useful for transition metal oxides.

The parameters for nearest and next nearest neighbor hopping (defined in Eqs. (3) and (8)-(13)) which we obtain for the ideal cubic structure with lattice constant $a_0 = 3.935 \text{ \AA}$ are $t = 0.655 \text{ eV}$ and $t' = 0.035 \text{ eV}$. The Hund’s rule and JT coupling constants (defined in Eqs. (4)-(5)) which we obtain from our analysis are $J = 1.34 \text{ eV}$ and $\lambda = 1.64 \text{ eV/\AA}$. Our value of $J = 1.34 \text{ eV}$ for the Hund’s coupling is in excellent agreement with the exchange splitting $2J = 2.7 \text{ eV}$ derived from x-ray absorption measurements,³¹ and agrees well with previous LSDA calculations.^{19,27} On the other hand, the strength of the JT coupling λ obtained in this work is smaller than what has been concluded from x-ray absorption measurements in Ref. 31. It is also smaller compared to various other values obtained previously from (mostly less elaborate) fits of similar TB models to LSDA or LSDA+ U band-structure calculations.^{19,20,21,32}

Popovic and Satpathy used a fitting procedure very similar to the one presented here, and obtained a JT coupling strength of $\lambda = 2.8 \text{ eV/\AA}$ (in our notation), compared to $\lambda = 1.64 \text{ eV/\AA}$ obtained in the present work.²⁰ We ascribe this difference to the use of the atomic sphere approximation (ASA) in the LSDA calculation of Ref. 20. In the ASA the crystal volume is represented by an arrangement of overlapping “atomic spheres”.³³ This overlap introduces an error, which furthermore depends on the amplitude of the JT distortion (since the JT distortion changes the overlap between the atomic spheres) and thus can have a pronounced effect on λ .

Ahn and Millis used a TB model very similar to the one used in this work, except that they didn’t include the effect of next-nearest neighbor hopping.¹⁹ They obtained a value of $\lambda = 3.38 \text{ eV/\AA}$ by simultaneously fitting 15 energies at 4 different high symmetry k -points to a previous LSDA calculation for the fully distorted antiferromagnetically ordered case. It is not obvious how sensitive such a simultaneous root mean square fit of all the model parameters is to the exact value of λ , but we expect that

the neglect of next nearest neighbor hopping will lead to a renormalization of the other parameters of the TB model in order to account for the missing dispersion due to the next-nearest neighbor hopping.

A value of $\lambda = 2.85 \text{ eV}/\text{\AA}$ was obtained by Yin et al.²¹ by calculating the dependence of several quantities on the amplitude of the JT distortion. This dependence was first obtained from LSDA+ U calculations within a Wannier function representation, and then compared to the corresponding results calculated for a model Hamiltonian including electron-electron interactions within the Hartree-Fock approximation. As in the case of Ref. 19 discussed above, it is not clear how sensitive this simultaneous fit of all parameters in the model Hamiltonian is to moderate changes in λ .

In contrast, the fitting procedure described in this work isolates the effect of each term in the Hamiltonian (Eq. (2)) and thus allows to obtain each parameter independently from all others. In particular, it becomes clear from our calculated band-structure shown in Fig. 8, that the JT distortion does not lead to a rigid splitting of the e_g bands, but that instead it has only subtle, albeit rather important effects on band crossings at certain k -points in the Brillouin zone. The reason for this is that the JT Hamiltonian H_{JT} in Eq. (5) for $Q^x \neq 0$ and staggered order does not commute with the kinetic energy term in Eq. (3), and that due to the relatively small value $\lambda Q_0^x \approx 0.25 \text{ eV}$ the hopping energies are dominant, so that in general the effect of the JT distortion is only visible as second order shifts in the energy. In other words, at a generic k -point the states picked out by the hopping term are not the eigenstates of the JT distortion. This suggests that the straightforward interpretation of peak splittings in the x-ray absorption spectra of Ref. 31 as a direct consequence of the JT distortion is not necessarily justified.

Finally, our analysis enables us to clearly identify the limitations of the effective two band e_g TB description of manganite systems. Our TB analysis was successful because in LaMnO₃ within LSDA the e_g bands are well-separated from the oxygen $2p$ bands, and neither the JT distortion nor the magnetic order change this energy spacing, and thus the value of the effective hopping, significantly. The dependence of the effective hop-

ping parameters on the energetic distance between the Mn e_g and the O $2p$ states (see Eq. (1)) is visible as a 15-20% difference between the majority-spin and the minority-spin bandwidths and dispersion in the ferromagnetic LSDA calculation for the cubic structure (see Sec. IIIB), and also in the high-lying bands of the antiferromagnetic LSDA band-structure shown in Fig. 6. However, in cases where the e_g and O $2p$ bands overlap in energy, such as for example in our LSDA+ U calculation for the purely JT distorted structure shown in Fig. 10, the effective e_g TB analysis fails, and the O $2p$ levels have to be taken into account explicitly.

The energy shift of the occupied d states relative to the oxygen p states within the LSDA+ U method is mainly caused by the so-called “double-counting correction”, which attempts to correct for those contributions of the electron-electron interaction that are accounted for in both the LSDA and the local Hartree-Fock (“+ U ”) treatment. Since the double-counting correction is notoriously ill-defined, this raises the question of whether such level shifts due to the electron-electron interaction and the resulting substantial renormalization of the effective hopping parameters are real effects, or whether this is an artifact of the LSDA+ U scheme, which only accounts for the static (mean-field) electron-electron interaction between the transition metal d states, while leaving the O $2p$ states unchanged (we point out that the same problem is also present within an LDA+DMFT treatment of electronic correlations). Optical evidence (see Ref. 34) suggests that the O $2p$ bands in manganites are located about 4eV below the Fermi level, consistent with the LSDA result, but more detailed investigations of the energy separation between the Mn e_g and O $2p$ bands will be useful for future studies.

Acknowledgments

This work was supported by the MRSEC Program of the National Science Foundation under award number DMR-0213574 (C.E.) and by the Department of Energy under grant number ER-46169 (A.J.M. and C.L.).

* Electronic address: ederer@phys.columbia.edu

¹ G. H. Jonker and J. H. Van Santen, *Physica* **16**, 337 (1950).

² E. O. Wollan and W. C. Koehler, *Phys. Rev.* **100**, 545 (1955).

³ J. M. D. Coey, M. Viret, and S. von Molnár, *Adv. Phys.* **48**, 167 (1999).

⁴ Y. Tokura, ed., *Colossal Magnetoresistive Oxides* (Gordon and Breach, 2000).

⁵ E. Dagotto, T. Hotta, and A. Moreo, *Phys. Rep.* **344**, 1 (2001).

⁶ S. Jin, T. H. Tiefel, M. McCormack, R. A. Fastnacht,

R. Ramesh, and L. H. Chen, *Science* **264**, 413 (1994).

⁷ P. Norby, I. G. K. Andersen, E. K. Andersen, and N. H. Andersen, *J. Solid State Chemistry* **119**, 191 (1995).

⁸ J. B. A. A. Elemans, B. Van Laar, K. R. Van der Veen, and B. O. Loopstra, *J. Solid State Chemistry* **3**, 238 (1971).

⁹ J. Kanamori, *J. Appl. Phys. (Suppl.)* **31**, 14S (1960).

¹⁰ P. M. Woodward, *Acta Cryst. B* **53**, 32 (1997).

¹¹ P. Hohenberg and W. Kohn, *Phys. Rev.* **136**, B864 (1964).

¹² W. Kohn and L. J. Sham, *Phys. Rev.* **140**, A1133 (1965).

¹³ O. Gunnarsson, O. K. Andersen, O. Jepsen, and J. Zaanen, *Phys. Rev. B* **39**, 1708 (1989).

- ¹⁴ M. S. Hybertsen, M. Schlüter, and N. E. Christensen, Phys. Rev. B **39**, 9028 (1989).
- ¹⁵ W. E. Pickett and D. J. Singh, Phys. Rev. B **53**, 1146 (1996).
- ¹⁶ S. Satpathy, Z. S. Popovic, and F. R. Vukajlović, Phys. Rev. Lett. **76**, 960 (1996).
- ¹⁷ I. Solovyev, N. Hamada, and K. Terakura, Phys. Rev. Lett. **76**, 4825 (1996).
- ¹⁸ K. Terakura, I. V. Solovyev, and H. Sawada, in *Colossal Magnetoresistive Oxides*, edited by Y. Tokura (Gordon and Breach, 2000), pp. 119–148.
- ¹⁹ K. H. Ahn and A. J. Millis, Phys. Rev. B **61**, 13545 (2000).
- ²⁰ Z. Popovic and S. Satpathy, Phys. Rev. Lett. **84**, 1603 (2000).
- ²¹ W.-G. Yin, D. Volja, and W. Ku, Phys. Rev. Lett. **96**, 116405 (2006).
- ²² P. E. Blöchl, Phys. Rev. B **50**, 17953 (1994).
- ²³ G. Kresse and J. Furthmüller, Phys. Rev. B **54**, 11169 (1996).
- ²⁴ G. Kresse and D. Joubert, Phys. Rev. B **59**, 1758 (1999).
- ²⁵ We use the notation of Ref. 26 to denote the high-symmetry points within cubic, tetragonal, and orthorhombic Brillouin zones.
- ²⁶ C. J. Bradley and A. P. Cracknell, *The mathematical theory of symmetry in solids* (Oxford University Press, 1972).
- ²⁷ Y. Yamasaki, S. Miyasaka, Y. Kaneko, J.-P. He, T. Arima, and Y. Tokura, Phys. Rev. Lett. **96**, 207204 (2006).
- ²⁸ A. Yamasaki, M. Feldbacher, Y.-F. Yang, O. K. Andersen, and K. Held, Phys. Rev. Lett. **96**, 166401 (2006).
- ²⁹ V. I. Anisimov, F. Aryasetiawan, and A. I. Liechtenstein, J. Phys.: Condens. Matter **9**, 767 (1997).
- ³⁰ S. L. Dudarev, G. A. Botton, S. Y. Savrasov, C. J. Humphreys, and A. P. Sutton, Phys. Rev. B **57**, 1505 (1998).
- ³¹ D. S. Dessau and Z.-X. Shen, in *Colossal Magnetoresistive Oxides*, edited by Y. Tokura (Gordon and Breach, 2000), pp. 149–185.
- ³² Note that different conventions for the JT coupling are used throughout the literature, so that care must be taken when comparing values from different sources.
- ³³ O. K. Andersen, Solid State Commun. **13**, 133 (1973).
- ³⁴ M. Quijada, J. Černe, J. R. Simpson, H. D. Drew, K. H. Ahn, A. J. Millis, R. Shreekala, R. Ramesh, M. Rajeswari, and T. Venkatesan, Phys. Rev. B **58**, 16093 (1998).